SATELLITE & MESOMETEOROLOGY RESEARCH PROJECT

Department of the Geophysical Sciences
The University of Chicago

AIRCRAFT, SPACECRAFT, SATELLITE, AND RADAR OBSERVATIONS OF HURRICANE GLADYS, 1968

by

R. Cecil Gentry
National Hurricane Research Laboratory

Tetsuya T. Fujita
University of Chicago

and

Robert C. Sheets
National Hurricane Research Laboratory

SMRP Research Paper

Number 83
May 1970

MESOMETEOROLOGY PROJECT --- RESEARCH PAPERS

1.* Report on the Chicago Tornado of March 4, 1961 - Rodger A. Brown and Tetsuya Fujita

2.* Index to the NSSP Surface Network - Tetsuya Fujita

3.* Outline of a Technique for Precise Rectification of Satellite Cloud Photographs - Tetsuya Fujita

4.* Horizontal Structure of Mountain Winds - Henry A. Brown

5.* An Investigation of Developmental Processes of the Wake Depression Through Excess Pressure Analysis of Nocturnal Showers - Joseph L. Goldman

6.* Precipitation in the 1960 Flagstaff Mesometeorological Network - Kenneth A. Styber

7.** On a Method of Single- and Dual-Image Photogrammetry of Panoramic Aerial Photographs - Tetsuya Fujita

8. A Review of Researches on Analytical Mesometeorology - Tetsuya Fujita

9.* Meteorological Interpretations of Convective Nephsystems Appearing in TIROS Cloud Photographs - Tetsuya Fujita, Toshimitsu Ushijima, William A. Hass, and George T. Dellert, Jr.

10.* Study of the Development of Prefrontal Squall-Systems Using NSSP Network Data - Joseph L. Goldman

11. Analysis of Selected Aircraft Data from NSSP Operation, 1962 - Tetsuya Fujita

12. Study of a Long Condensation Trail Photographed by TIROS I - Toshimitsu Ushijima

13. A Technique for Precise Analysis of Satellite Data; Volume I - Photogrammetry (Published as MSL Report No. 14) - Tetsuya Fujita

14. Investigation of a Summer Jet Stream Using TIROS and Aerological Data - Kozo Ninomiya

15. Outline of a Theory and Examples for Precise Analysis of Satellite Radiation Data - Tetsuya Fujita

16. Preliminary Result of Analysis of the Cumulonimbus Cloud of April 21, 1961 - Tetsuya Fujita and James Arnold

17. A Technique for Precise Analysis of Satellite Photographs - Tetsuya Fujita

18.* Evaluation of Limb Darkening from TIROS III Radiation Data - S.H.H. Larsen, Tetsuya Fujita, and W.L. Fletcher

19. Synoptic Interpretation of TIROS III Measurements of Infrared Radiation - Finn Pedersen and Tetsuya Fujita

20.* TIROS III Measurements of Terrestrial Radiation and Reflected and Scattered Solar Radiation - S.H.H. Larsen, Tetsuya Fujita, and W.L. Fletcher

21. On the Low-level Structure of a Squall Line - Henry A. Brown

22.* Thunderstorms and the Low-level Jet - William D. Bonner

23.* The Mesoanalysis of an Organized Convective System - Henry A. Brown

24. Preliminary Radar and Photogrammetric Study of the Illinois Tornadoes of April 17 and 22, 1963 - Joseph L. Goldman and Tetsuya Fujita

25. Use of TIROS Pictures for Studies of the Internal Structure of Tropical Storms - Tetsuya Fujita with Rectified Pictures from TIROS I Orbit 125, R/O 128 - Toshimitsu Ushijima

26. An Experiment in the Determination of Geostrophic and Isallobaric Winds from NSSP Pressure Data - William Bonner

27. Proposed Mechanism of Hook Echo Formation - Tetsuya Fujita with a Preliminary Mesosynoptic Analysis of Tornado Cyclone Case of May 26, 1963 - Tetsuya Fujita and Robbi Stuhmer

28. The Decaying Stage of Hurricane Anna of July 1961 as Portrayed by TIROS Cloud Photographs and Infrared Radiation from the Top of the Storm - Tetsuya Fujita and James Arnold

29. A Technique for Precise Analysis of Satellite Data, Volume II - Radiation Analysis, Section 6. Fixed-Position Scanning - Tetsuya Fujita

30. Evaluation of Errors in the Graphical Rectification of Satellite Photographs - Tetsuya Fujita

31. Tables of Scan Nadir and Horizontal Angles - William D. Bonner

32. A Simplified Grid Technique for Determining Scan Lines Generated by the TIROS Scanning Radiometer - James E. Arnold

33. A Study of Cumulus Clouds over the Flagstaff Research Network with the Use of U-2 Photographs - Dorothy L. Bradbury and Tetsuya Fujita

34. The Scanning Printer and Its Application to Detailed Analysis of Satellite Radiation Data - Tetsuya Fujita

35. Synoptic Study of Cold Air Outbreak over the Mediterranean using Satellite Photographs and Radiation Data - Aasmund Rabbe and Tetsuya Fujita

36. Accurate Calibration of Doppler Winds for their use in the Computation of Mesoscale Wind Fields - Tetsuya Fujita

37. Proposed Operation of Intrumented Aircraft for Research on Moisture Fronts and Wake Depressions - Tetsuya Fujita and Dorothy L. Bradbury

38. Statistical and Kinematical Properties of the Low-level Jet Stream - William D. Bonner

39. The Illinois Tornadoes of 17 and 22 April 1963 - Joseph L. Goldman

40. Resolution of the Nimbus High Resolution Infrared Radiometer - Tetsuya Fujita and William R. Bandeen

41. On the Determination of the Exchange Coefficients in Convective Clouds - Rodger A. Brown

* Out of Print
** To be published

(Continued on back cover)

SATELLITE AND MESOMETEOROLOGY RESEARCH PROJECT
Department of the Geophysical Sciences
The University of Chicago

AIRCRAFT, SPACECRAFT, SATELLITE, AND RADAR OBSERVATIONS OF HURRICANE GLADYS, 1968

by
R. Cecil Gentry
National Hurricane Research Laboratory

Tetsuya T. Fujita
The University of Chicago
and

Robert C. Sheets
National Hurricane Research Laboratory

SMRP Research Paper No. 83
May 1970

The part of this research performed at the University of Chicago has been sponsored by the U. S. Weather Bureau, ESSA under grant E22-69-70(G).

AIRCRAFT, SPACECRAFT, SATELLITE, AND RADAR OBSERVATIONS OF HURRICANE GLADYS, 1968[1]

by

R. Cecil Gentry
National Hurricane Research Laboratory

Tetsuya T. Fujita
University of Chicago

and

Robert C. Sheets
National Hurricane Research Laboratory

ABSTRACT

Hurricane Gladys, 17 October 1968, is studied with data collected by the Apollo 7 manned spacecraft, ESSA's especially instrumented aircraft, weather search radar, the ATS III and ESSA 7 satellites and the conventional weather networks. This is the first time data from all of these observing tools have been used to study the structure and dynamics of a hurricane. Techniques used in computing and integrating the various types of data are described and illustrated.

A dominant feature of this immature hurricane was a large cloud which provided a major link between the low and high level circulations of the storm. Evidence is presented to suggest this type of cloud and its attendant circulation are features representative of tropical cyclones passing from the tropical storm to the hurricane stage.

1. Introduction

Hurricane Gladys and Apollo 7, the manned spacecraft, by coincidence, were over the Gulf of Mexico at the same time on 17 October 1968. Research aircraft, land based radar, weather satellites, and the conventional weather data networks, by plan, were collecting data on Hurricane Gladys on this same day. The men in Apollo 7 used Gladys as a target of opportunity and obtained some wonderful pictures of the storm. The

[1]Portions of this research performed at the University of Chicago have been sponsored by ESSA under Grant NSSL- E-22-41-69.

combination of these circumstances provided us with a rare opportunity to use data from a number of sources to study the structure and dynamics of a tropical cyclone.

The list of observing tools trained on Gladys is indeed impressive. Two aircraft (one DC-6 and one B-57) from ESSA's Research Flight Facility flew in the hurricane. ESSA's WSR-57 radars at Tampa, Key West and Miami observed the storm from the outside; ATS III and ESSA 7 satellites took pictures from above; the conventional surface and upper air weather networks of the United States and neighboring countries collected data on the ambient conditions; and during a 2-minute period about 1530 GMT, the Apollo 7 crew took 5 color pictures of the storm. The research aircraft crews took pictures of the clouds every 2 to 5 seconds, photographs of the radar scopes every sweep, and measurements of wind direction, speed, temperature and D-value every second.

Hurricanes have been studied in the past with land based radar data (Wexler, 1947; Kessler and Atlas, 1956; and Newman and Boyd, 1962), with aircraft data (LaSeur and Hawkins, 1963; and Gentry, 1964, 1967) and a combination of aircraft and satellite data (Hawkins and Rubsam, 1968a, 1968b; and Fett, 1968). It is believed, however, that this is the first time so many observational tools were used in a single storm study.

Initially, we proposed to determine how best to integrate output from these various observational tools in a study of a weather phenomena. In the process of the study we learned several interesting things about an immature hurricane and gained further insight of the mechanism by which the convective and synoptic scales interact to change a tropical storm into a hurricane. In this paper, therefore, we present examples of the various types of data collected and analyzed, show how they complement each other, and discuss the structure and dynamics of the developing storm.

The Apollo 7 picture of Hurricane Gladys (Fig. 1) is dominated by a large circular shaped cloud which was near but to the north of the hurricane center. Analyses showed this to be one of the most interesting features of the storm and an essential link in the radial-vertical circulation of mass through the hurricane. We called it the circular exhaust cloud (CEC) and will discuss its formation and evolution in some detail.

a. History of Hurricane Gladys

A disturbed weather area formed on the ITC near San Andres in the western Caribbean on 13 October. After drifting slowly north-northwestward it intensified into tropical storm Gladys on 15 October (Sugg and Herbert, 1969). Gladys reached hurricane intensity before reaching the south coast of Cuba. Although it weakened some while crossing that country, it was near hurricane force when it passed into the Florida Straits area late on 16 October (Fig. 2).

Gladys moved in a generally northerly direction during the night of the 16th and the morning of the 17th. By 1500 GMT 17 October, it was centered about 130 n mi west-southwest of Tampa, Florida. Gladys, on this day, was of minimal hurricane intensity (maximum winds measured at 1770 ft. by aircraft were 64 knots), and had a minimum sea level pressure of 986 mb.

Gladys crossed northern Florida during the night of 18 October emerging on the east coast near St. Augustine about daybreak 19 October. It then moved northeastward over the Atlantic not far from the coastline and finally became extratropical as it merged with a cold front off the coast of Nova Scotia on 21 October.

2. Analysis of Apollo Pictures Together with WSR-57 Pictures

Since the Apollo 7 pictures showing Gladys on 17 October 1968 reveal the fine structure of a weak hurricane presumably well, they have been analyzed by several investigators with varying degrees of precision. Notably, the cover picture of the AMS Bulletin, February 1969, and the qualitative study by Soules and Nagler (1969) revealed the potential values of detailed study of 70-mm color pictures taken from an earth-orbiting platform.

In order to carry out an accurate photogrammetric analysis of five usable pictures, each negative was enlarged to a size with a principal distance of f = 320 mm. The print size corresponding to this focal distance is about 9" x 9". Fortunately all are high oblique pictures, permitting us to compute the picture tilt from

$$\tau = 90° - (\delta_H + \epsilon_H) \qquad (2.1)$$

where τ is the tilt, δ_H, the dip of the horizon computed from the Apollo height and the earth's radius, and ϵ_H the radial angle[2] of the horizon on the principal line. After computing each tilt, picture No. 1 showing at least 30 identifiable landmarks was used in transferring these landmarks to a height grid on a zenithal equidistant (ZE) projection of 1:2,500,000 scale. The transfer procedure by means of tilt-and height-grid system is described by Fujita (1963) in a text of satellite photogrammetry. By placing landmarks in a ZE projection sheet onto a 2,500,000 map an excellent fit between landmarks on the sheet and the map was achieved, thus determining the exposure subpoint and the azimuth of the principal line to be 118° (See Fig. 3).

Although picture No. 2 included no landmarks whatsoever, approximately 50 cloud shadows plotted on the $1:2.5X10^6$ map from the previous picture were used as if they were small islands floating over the Gulf. The shadow movement between exposure times of pictures 1 and 2 about 30 sec is small enough to be neglected. This bridge method premitted us to determine photogrammetric quantities from one picture to the next.

To safeguard against amplification of errors in this bridge method, positions of small radar echoes from Tampa and Key West were also used. By doing this, we were able to use small echoes as positions of small precipitating clouds. Thus we carried on successive photogrammetric analyses to determine the final photogrammetric data in Fig. 3. It should be noted that the final track of Apollo 7 was obtained by drawing the best fit great circle which could be up to one nautical mile off the predetermined exposure subpoints. The distance in geocentric angle between pictures 1 and 5 subpoints was about 8 degrees corresponding to a 2-min travel time by Apollo 7, resulting in an estimated average picture-taking interval of 30 sec.

Unlike gridding procedure of televised satellite pictures, it is necessary to take cloud heights into consideration when drawing exact longitude and latitude circles on an Apollo photograph. Since cloud heights were not known initially, we computed grid lines at sea level as a first step toward more advanced analyses. Sea-level grid lines thus obtained were superimposed upon picture No. 4 with a 73.0° tilt (see Fig. 4). Locations

---

[2] Radial angle is defined as the angle between an object and the principal point viewed from the perspective center of a picture.

of selected cities such as Miami, Key West, and Havana are identified in the picture.

The resolution of the picture is so high that even towering cumuli beyond Cuba can clearly be identified. A well-defined cloud band extends from near Cuba to the west of Key West and spirals into the hurricane area. The hurricane center at 1531 determined from WSR-57 radars at Key West and Tampa appears near the right edge of the CEC in the picture. In order to determine the exact relationship between the CEC and the hurricane center, we must project its circular rim down to sea level. Such a projection will shift the cloud position considerably toward the camera. Unfortunately, however, the amount of shift cannot be computed without knowing the height of the CEC above sea level.

Computation of cloud height from aerial or satellite pictures can be performed through standard photogrammetric techniques if stereo-pair pictures are available. An attempt was made to compute cloud heights from pairs numbered 1 and 2, 2 and 3, etc., but it turned out to be unsuccessful. One reason was that the large distance between Apollo and the clouds prevented making height computations by this technique with errors less than 500 m.

Recently Fujita (1969) developed a method of computing cloud heights from the length of a vector on the picture connecting a cloud with its shadow. It would be necessary to refer to the original paper for detail. In brief, the equations used for the computation permit us to obtain the cloud height, h, from

$$h = \lambda \Delta s, \tag{2.2}$$

where Δs is the length of the vector connecting the shadow with the cloud and λ, a non-dimensional quantity which can be contoured on an image. This quantity is computed by

$$\lambda = \frac{\mu D}{f} \cdot \frac{\cos \zeta^*}{\sin \psi} \tag{2.3}$$

where D is the distance from camera to shadow, f, the principal distance, ζ^*, the solar

zenith angle at the shadow, μ, the scattering angle from the sun to Apollo onto the shadow, and ψ, the perspective parameter which decreases outward from the principal point or the picture center where $\mu = 1.0$.

After computing λ by putting proper parameters through a computer, we draw isolines of λ on an image. All that is then required to obtain cloud heights is to measure the shadow-to-cloud distances and multiply by λ. So long as a cloud and its shadow are identified in a picture, the height computation takes no more than 10 sec per cloud. If we measure shadow lengths with 0.2 mm accuracy, the error in cloud height will be about 500 m at the distance of Cuba in Fig. 4. As we approach the lower portion of the picture, 200 m accuracy in the cloud height estimate can be obtained.

An example of a composite prepared from the analyzed Apollo picture and WSR-57 radar pictures taken simultaneously at Key West, Miami, and Tampa is presented in Fig. 5. Black areas represent radar echoes which are enclosed by cloud boundaries as determined from Apollo pictures. Heights in kilometers of cloud tops corresponding to these echoes are shown. The areas of clouds extending above the 10 km level are stippled.

The height of the CEC at its edge was estimated to be 12 km MSL. Its top would be as high as 14 km. Streaks of high clouds indicate a pattern of outflow stimulated by the expansion of the CEC. A pronounced cloud or echo band extending toward Cuba was made of cellular echoes with the cloud-top heights reaching 3 to 10 km MSL. Most of them, however, had tops at about 5 km. No anvils were seen to originate from these cells. The axis of these clouds appeared to be almost vertical when viewed from the northwest.

The location of the CEC relative to the hurricane center was established after determining its height to be 12 km MSL. It was then learned that the CEC was located over the region of converging echo bands to the north of the hurricane center which is likely to be a spot on the eyewall where convergence is most significant.

This example of analysis demonstrates that proper photogrammetric technique permits us to analyse Apollo pictures with high accuracy. Pictures can be used in mapping clouds together with radar echoes. Cloud heights can also be computed from cloud shadows so long as we see them in a picture; and the accuracy of height computation is good enough for research on the fine structure of hurricanes.

3. Aircraft Data

a. Cloud Structure

The cloud structure as observed from the research aircraft generally reflected the same characteristics as shown by the Apollo pictures. The cirrus shield was much smaller than that usually associated with more mature or intense hurricanes. Most of the cirrus clouds were over the eastern half of the storm and even here were generally broken to occasionally scattered. The low level flight pattern was confined to within 70 n mi of the storm center (Figs. 6 and 7) except when entering and exiting the storm area. During the circumnavigation of the storm at a radius of 65 n mi, the aircraft was clear of clouds more than half the time. Only occasionally did the low level clouds observed indicate much vertical development and very few middle level clouds were observed. During the circumnavigation at a radius of 30 n mi and the two radial passes, the only strong convection encountered was in the region of the CEC, north of the storm center. A flight pattern similar to that shown in Figure 7 was completed at a level of 6,400 feet (not illustrated) and similar cloud conditions were observed.

The ESSA Research Flight Facility B-57 aircraft flew the pattern illustrated in Fig. 8 over the storm at an altitude near 44,000 feet during the period of the Apollo pictures and the low level flight. The cloud tops approached the aircraft level only in the northeast quadrant, the CEC area, and in a band approximately 60 n mi south of the storm center. The CEC showed a very distant hard core convective area protruding through the general cirrus outflow level (Fig. 9).

Fig. 9a shows the CEC as observed from the DC-6 aircraft at an altitude of 1770 feet while Figs. 9b and 9c show the area of the CEC recorded by the forward oriented 16 mm camera in the B-57 at 44,000 feet. Fig. 9d shows the CEC as observed on the scope of the vertically oriented RDR 3.2 cm radar system in the DC-6 aircraft. The radar system scans a plane normal to the aircraft heading and was being operated in the isoechomode. The narrow clear band slightly below the center of the scope extending both right and left separates the sea return from the cloud echoes above. The most intense portion of the echo from the CEC is the dark area surrounded by the light area centered

just to the right of the center of the scope. The range markers are at 5 n mi intervals and the center of the scope is at the aircraft altitude, 6,400 ft. The CEC echo then extends to approximately 35,000 ft.

b. Low Level Wind Field

The winds measured during the flight at the 1770 ft level have been composited with each wind positioned relative to the center of the hurricane. If we assume that the storm was in a steady state during the 3.5 hr needed to collect the data, we can treat these winds as though they were all measured at the same time. We did this in preparing the streamline and isotach analysis of the winds at 1770 ft shown in Fig. 7. Maximum wind speeds exceeding 60 kt were recorded within 50 n mi of the storm center north and east of the circulation center. The typical spiralling inward of flow at this level is illustrated by the streamline analysis.

This analyzed wind field was used in computing the divergence. The winds used were interpolated from the analyses for a 10 n mi grid spacing and smoothed by a 9 point smoothing routine. The divergence field computed from these smoothed winds shows a maximum of convergence of $1.5 \times 10^{-4}\ sec^{-1}$ in the vicinity of the CEC (Fig. 10). Convergence was typical of most of the eastern half of the storm but an area of divergence at a radius of 30 to 40 n mi extended from the western side of the storm around toward the storm center in the south and south-east sides. These latter areas were mostly free of major cloud buildups (Fig. 5).

It is interesting to note the degree of correspondence between the principal cloud features of Gladys and the vertical motions one may infer from the data in Fig. 7 and 10, even though one may certainly question the accuracy of the divergence values calculated in the described manner. The most notable features of the cloud structure have already been mentioned, that is, the CEC and the relatively low amount of total convective cloudiness for Gladys as compared with the typical hurricane. The coincidence of the area of maximum convergence with the location of the CEC has already been noted. The relatively low amount of total cloudiness may be attributed to the likewise relatively small net convergence for the storm area (for example, inside the 60 n mi radius).

The net divergence as computed from circumnavigations at levels below 3500 ft at approximately 60 n mi is given for a few tropical cyclones in Table 1. These values were computed by

$$\overline{D_f} = \frac{1}{A_f} \oint V_n \, dS \qquad (3.1)$$

where $\overline{D_f}$ is the mean divergence for the area, A_f is the area bounded by the circumnavigation portion of the flight (approximately the area inside 60 n mi radius), V_n is either the normal or radial component of the wind, and S is the curve representing the line of flight. The net divergence in Gladys was a full order of magnitude less than in the other storms. This could account for the relatively low amount of intense convective clouds.

This relatively weak convergence field may also be either the cause or another effect of Gladys being very slow to intensify. Gladys was passing over warm water at the time (McFadden, 1970). The sea surface temperatures were above 28 C which is warm enough to supply fuel for an intense hurricane.

Table 1. Net Divergence in Tropical Cyclones Computed from Flight Winds.

Name	Date	Flight Level (ft)	Divergence (10^{-5} sec^{-1})	Approx. Max. Winds kt
Janice	8 Oct. 1958	1600	-11	55
Betsy	1 Sept. 1965	500	-17	80
Betsy	1 Sept. 1965	1000	-26	80
Betsy	3 Sept. 1965	3240	-16	125
Betsy	5 Sept. 1965	2000	-11	125
Gladys	17 Oct. 1968	1770	- 1.3	64

c. Vertically Oriented Radar Cross Sections

Figures 11A and 11B show composites of radar echoes from the vertically oriented 3.2 cm radar, profiles of wind speeds relative to the moving storm center, temperatures, and relative humidities. All are plotted versus radial distance from the storm center for a north-south oriented pass through the storm. The vertically oriented radar composites were obtained from pictures similar to that shown in Fig. 9d which were taken at 16 sec intervals.

The major echo on the north side of the storm in Figure 11A is associated with the CEC during its earlier stages. As can be seen, there are few radar echoes on this pass and only the CEC echo exceeds 16,000 ft in height. The other passes through the storm showed essentially the same structure with only a few echoes outside the area of the CEC and these echoes showed little vertical development.

A later north-south pass is shown in Figure 11B and depicts the development of and spreading out of the echo associated with the CEC during the day. A series of horizontal radar composites similar to Fig. 5, were constructed using the Tampa and Key West WSR-57 and the airborne radar presentations. These composites (not illustrated), showed the development of the echoes associated with the CEC increasing with time and extending around the northeast and south sides of the eye by 1630 GMT. The major echoes remained in the northeast quadrant, and increased in size and intensity during the day. Many echoes were observed over the eastern and northern portions of the storm with some echoes located as much as 300 n mi from the storm center. At the same time, very few moderate or strong echoes were observed west and southwest of the storm center. This was quite similar to the radar structure observed during the previous day just after Gladys had passed over Cuba and was in the process of reforming (Sheets, 1969).

4. A Model of Circular Exhaust Clouds (CEC)

Based upon observational evidences, we shall discuss the characteristics of the circular exhaust cloud which dominated outer-space views of Hurricane Gladys on 17 October 1968.

It is rather unfortunate that no televised satellite pictures of Gladys were available concurrently with Apollo 7 pictures exposed between 1530 and 1531 GMT. ATS III spin-scan pictures were taken later at 1713, 1927, 1952, 2017, and 2107 GMT, as well as ESSA 7 pictures exposed at 1935 GMT. Combined analyses of these pictures revealed that the diameter of CEC increased significantly.

Table 2. Diameter of CEC Measured from Various Satellite Pictures Taken on 17 October 1968.

Time (GMT)	1530	1713	1927	1934	1952	2017
Diameter (km)	55	93	110	110	115	120
Determined by	Apollo 7	ATS III	ATS III	ESSA 7	ATS III	ATS III

These diameters as tabulated in Table 2 permit us to estimate the mean divergence inside the CEC at the height of its expanding leading edge. The mean divergence expressed by

$$\overline{D}_{CEC} = \frac{1}{A_{CEC}} \oint V_e \, dS \qquad (4.1)$$

where A_{CEC} denotes the horizontal area of the CEC, V_e, the component of expanding velocity normal to the edge segment, dS of the CEC. Under the assumption of a circular cloud with constant rate of expansion we may reduce Eq. (4.1) to

$$\tilde{\overline{D}}_{CEC} = \frac{2}{R} \cdot \frac{dR}{dt} = \frac{2}{\tilde{R}} \cdot \frac{\Delta R}{\Delta t} \qquad (4.2)$$

where R is the radius of the CEC and $\sim$ denotes the mean value averaged during the period Δt.

The mean divergence thus computed for a 1.7 hour period, 1530-1731 GMT turned out to be $17 \times 10^{-5} \text{sec}^{-1}$ while that for a 3.1 hour period 1713-2017 GMT was only

$5 \times 10^{-5}\ sec^{-1}$. These values indicate that the divergence at the CEC level decreased considerably. But the total expansion rate as defined by

$$\oint V_e\, dS = A_{CEC}\bar{D}_{CEC} \cong \pi R^2 \bar{D}_{CEC}$$

decreased from 2.8 $km^2\ sec^{-1}$ to 2.0 $km^2\ sec^{-1}$. This would mean that the total convective mass transport beneath the CEC remained almost unchanged for about five hours after Apollo 7 pictures were taken at 1530 GMT.

The displacement of the CEC as a whole is of extreme interest. The CEC center located some 35 km north-northeast of the hurricane center rotated in four hours by about 100 around the hurricane center. The rotation speed of the CEC relative to the storm center was therefore, only about 6 kt which is no more than 10% of the low-level flow directly beneath the CEC. It is likely that the motion of the CEC corresponds to that of the field of low-level convergence shown in Fig. 10. The maintenance and the motion of such a CEC-scale convergence area is closely related to the asymmetric nature of a hurricane.

While the CEC rotated very slowly around the hurricane center, WSR-57 radar from Tampa indicated that cellular echoes inside the CEC area were moving at the rate of about 30 kt, just about 50% of the low-level wind speed. Evidently, echoes either formed or intensified near the upwind edge of the CEC; meanwhile, continuous dissipation was taking place along the downwind edge.

A schematical cross section of the CEC including a convective tower was constructed in Fig. 12 in which the vertical and the horizontal velocities of the air inside the tower are given to the left and the right, respectively. Step by step computations revealed that it would take about 25 min for the inflow air at the cloud base to reach near the cloud top. According to Fujita and Grandoso's (1968) concept of a sliced cloud disc, the axis of a convective tower and trajectories of parcels occupying various parts of the tower are quite different. For instance, a parcel A near the cloud top must have entered the cloud base 25 min earlier. Its trajectory is shown by a tilted curve connecting a with A. The end points of successive trajectories departing from a through e at the cloud base determine the present shape of the tower axis A, B, ... F. It should be noted that the displacement rate of a, b, ... e is controlled by the propagation of the field of an impulse giving rise

to the vertical acceleration of uprising air. In order to gain some 5 m sec^{-1} vertical velocity within about a one km layer above the surface, the impulse should be identified as a convergence field of

$$\text{subcloud convergence} = 5 \text{ m sec}^{-1} / 1 \text{ km} = 500 \times 10^{-5} \text{ sec}^{-1} .$$

Despite the significant tilt of the trajectory of ascending air, the tower axis is maintained more or less in an upright position. The figure clearly indicates the major difference between trajectories and the tower axis.

While the maximum convergence beneath each tower is estimated to be about 500×10^{-5} sec^{-1} the overall convergence beneath the CEC shows a maximum of about 15×10^{-5} sec^{-1}. These values imply that the area of tower-scale convergence is only a few percent of that of CEC-scale convergence.

CEC in other hurricanes. The foregoing study suggests that a CEC could be formed where a CEC-scale convergence area is topped by a weak flow at the hurricane outflow level. Most weak hurricanes are characterized by such a structure. In order to find simular CECs in premature hurricanes, a number of ATS III pictures were examined. One of the best examples in hurricane Debbie of 16 August 1969 will be discussed.

As shown in Fig. 13, the first indication of a CEC was seen at 0952 GMT on the eyewall southwest of the hurricane center. The cloud identified by a letter "A" increased its diameter from 50 to 110 km in about two hours. The second CEC identified as D appeared at 1005Z in a pair. Then they grew and merged. A total of five CECs were spotted during early morning hours when the low angle of the sun permitted their easy identification.

In most cases the CEC started in the form of isolated point sources such as D at 1005 and C at 1018. These points grew into circular clouds with about a 20 km diameter in less than 15 min.

All CECs rotated around the hurricane center cyclonically at the rate of 23 kt for A, 20 kt for B, 16 kt for C, and 25 kt for D. The maximum windspeed of Debbie was

about 50 kt, indicating that the storm has not reached hurricane intensity yet. It is seen, from these data, that the CECs rotated at about one half of the tangentional windspeed of the parent storm. In the case of Gladys, however, the motion of the CEC was only about 10% of the maximum windspeed around the storm center. Further research on the wind and cloud motion in other storms is required in order to establish their dynamical relationship. Nevertheless the finding of a number of CECs in the development stage of Debbie is rather encouraging since we now feel that the CEC could be found in many other hurricanes.

5. Conclusions

Data collected for Hurricane Gladys 17 October 1968, by Apollo 7 manned spacecraft, aircraft of ESSA's Research Flight Facility, ATS III and ESSA 7 satellites, WSR-57 search radars and conventional weather networks have been integrated in this study of the storm. Description of the various types of data are provided and techniques for utilizing them are explained.

By using data from all the sources, it was practical to deduce features of the 3-dimension mass circulation through the hurricane and to gain new insight concerning the mechanisms by which a hurricane develops. The circular exhaust cloud which dominates the Apollo 7 pictures of the hurricane is an essential link in this 3-dimensional circulation and may be typical of the types of clouds developed in hurricane genesis situations.

REFERENCES

Fett, R. W., 1968: Some unusual aspects converning the development and structure of Typhoon Billie - July 1967. Mon. Wea. Rev., 96, 637-648.

Fujita, T., 1963: A technique for Precise Analysis for Satellite Data; Volume 1 - Photogrammetry Meteorological Satellite Laboratory Report 14, ESSA. 106 pp.

_____, and H. Grandoso, 1968: Split of a thunderstorm into anticyclonic and cyclonic storms and their motion as determined from numerical model experiments. J. of Atm. Sci., 25, 416-439.

_____, 1969: A method of computing cloud height from an Apollo picture using cloud shadows. To be printed as SMRP Report 82.

Gentry, R. C., 1964: A study of hurricane rainbands. Nat. Hurcn. Res. Proj. Rpt, 69, Weather Bureau. 85 pp.

_____, 1967: Structure of the upper troposphere and lower stratosphere in the vicinity of Hurricane Isbell, 1964. Papers in Meteorology and Geophysics, XVIII No. 4. Meteor. Res. Inst., Tokyo, 293-310.

Hawkins, H. F., and D. T. Rubsam, 1968: Hurricane Hilda, 1964, I. Genesis, as revealed by satellite photographs, conventional and aircraft data. Mon. Wea. Rev., 96, 428-452.

_____, and _____, 1968: Hurricane Hilda, 1964, II. Structure and budgets of the hurricane on October 1, 1964, Mon. Wea. Rev., 96, 617-636.

Kessler, E., and D. Atlas, 1956: Radar-synoptic analysis of Hurricane Edna, 1954. Geophys. Res. Pap., No. 50, Geophys. Res. Directorate, Bedford, Mass., 113 pp.

LaSeur, N. E. and H. R. Hawkins, 1963: An analysis of Hurricane Cleo (1958) based on data from research reconnaissance aircraft. Mon. Wea. Rev. 91, 694-709.

McFadden, J.D., 1970: Airborne investigation of the effects of hurricanes on the thermal structure of the surface layer of the ocean. Proceeding of Symposium on Investigations and Resources of the Caribbean Sea and Adjacent Regions, Willemstad, Curacao, N.A. 18-23 November 1968, to be published in 1970.

Neuman, S. and J. G. Boyd, 1962: Hurricane movement and variable location of high intensity spot in wall cloud radar echo, Mon. Wea. Rev. 90, 371-374.

Sheets, R. C., 1969: Preliminary Analysis of Cloud Physics Data Collected in Hurricane Gladys (1968), Project STORMFURY Annual Report 1968, Appendix D, D 1-11.

Soules, S. D. and K. M. Nagler, 1969: Two tropical storms viewed by Apollo 7. Bull. of A. M. S., 50, 58-65.

Sugg, A. and P. J. Hebert, 1969: The Atlantic hurricane season of 1968. Mon. Wea. Rev., 97, 225-239.

Wexler, H., 1947: Structure of hurricanes as determined by radar. Annals of the New York Academy of Sciences, 48 Art. 8, 821-844.

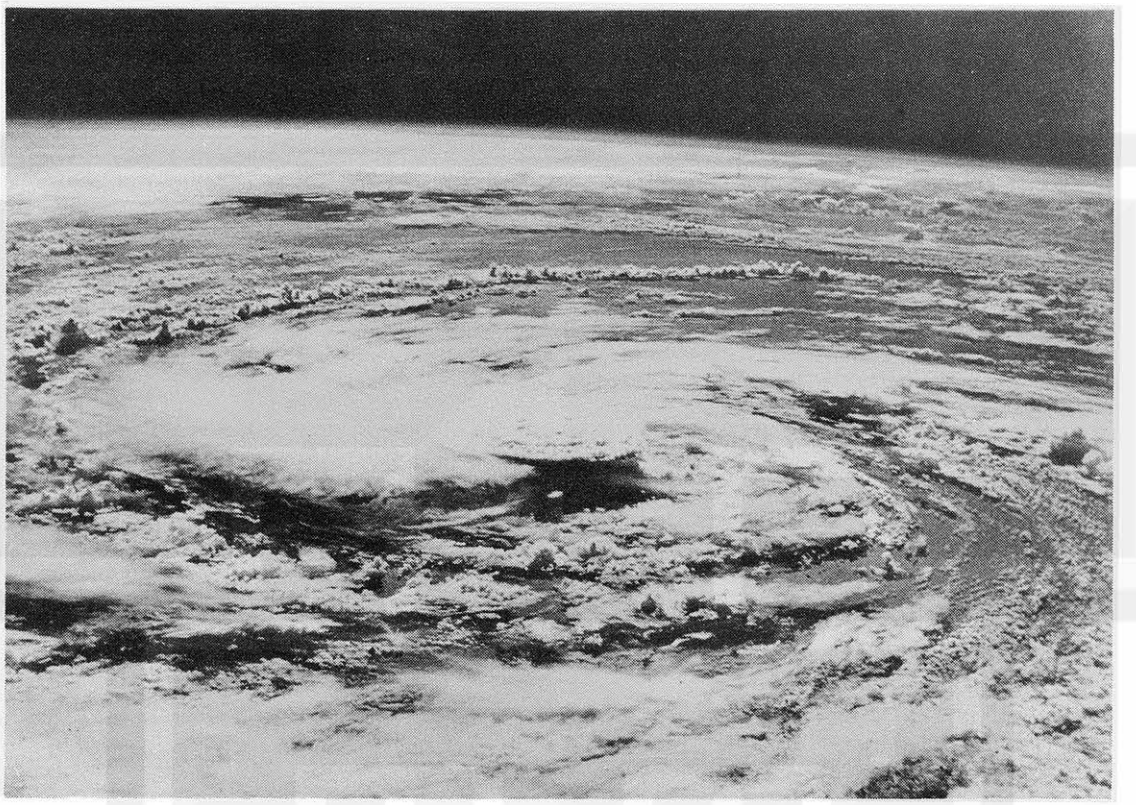

Fig. 1. Apollo-7 view of Hurricane Gladys at 1531 GMT 17 October 1968. A saucer-like cloud termed Circular Exhaust Cloud (CEC) is seen near the picture center some 500 km away. Although the CEC appears to be situated over the hurricane center, later analysis revealed that the center was located at the rear right edge of the CEC.

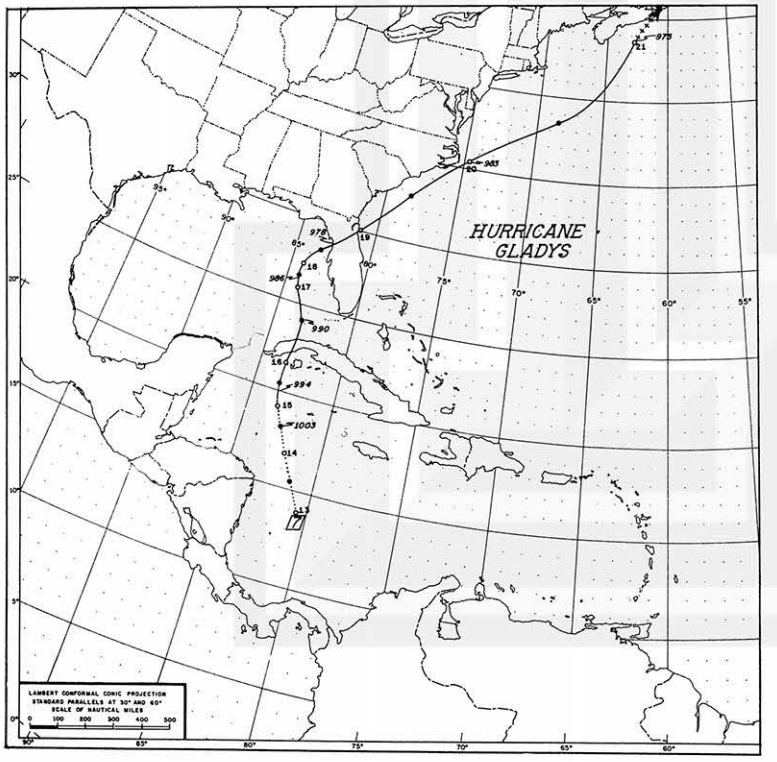

Fig. 2. Track of Hurricane Gladys 13-21 October 1968.

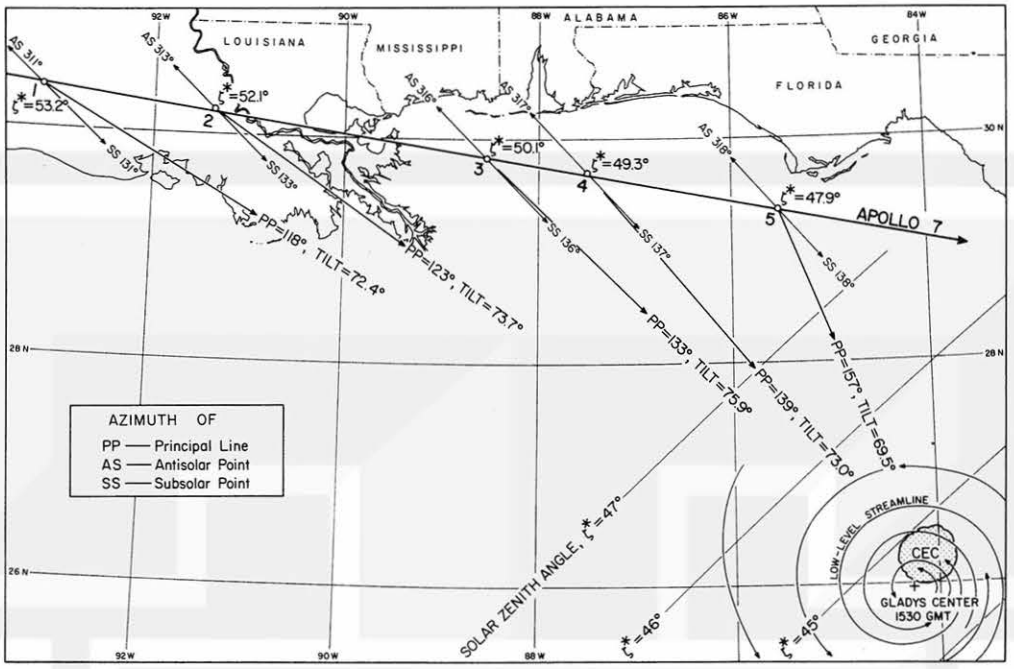

Fig. 3. Apollo 7 track determined from exposure subpoints of pictures 1 through 5 taken between 1530 and 1531 GMT from 99 to 100 nautical mile altitude. Sun angle computation indicates that Gladys was illuminated by the sun with solar zenith angle of about 45° from the direction of about 135° azimuth.

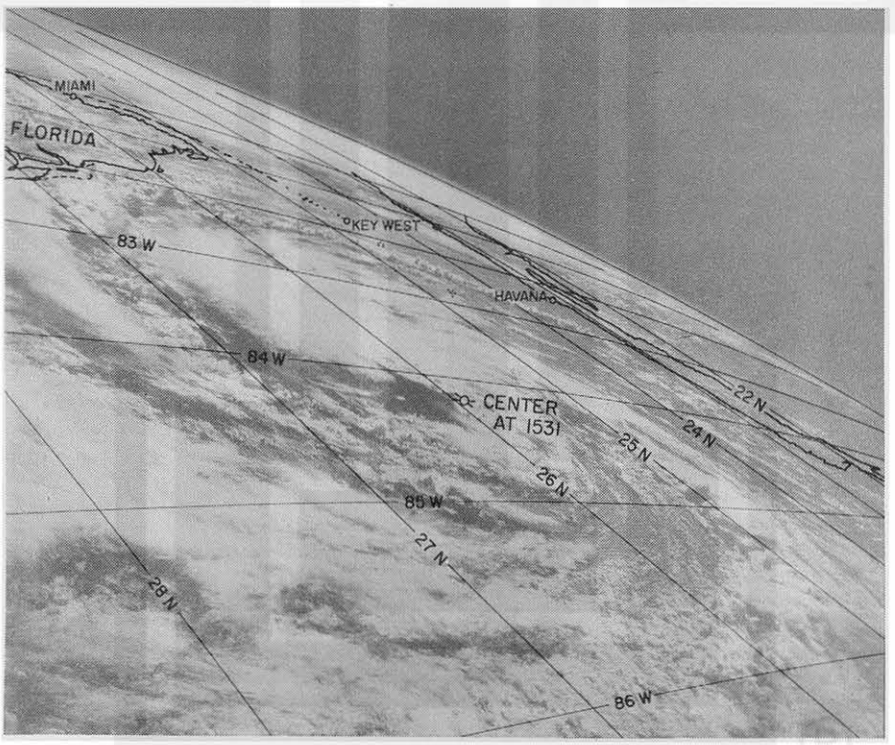

Fig. 4. Apollo 7 picture No. 4 with geographic grids at one-degree interval drawn at sea level. The picture principal line points toward 139° azimuth. The azimuth of the sun was 137° with the elevation angle of 40.7°. Thus the picture was taken facing toward the sun, resulting in the cloud shadows casting toward the observer.

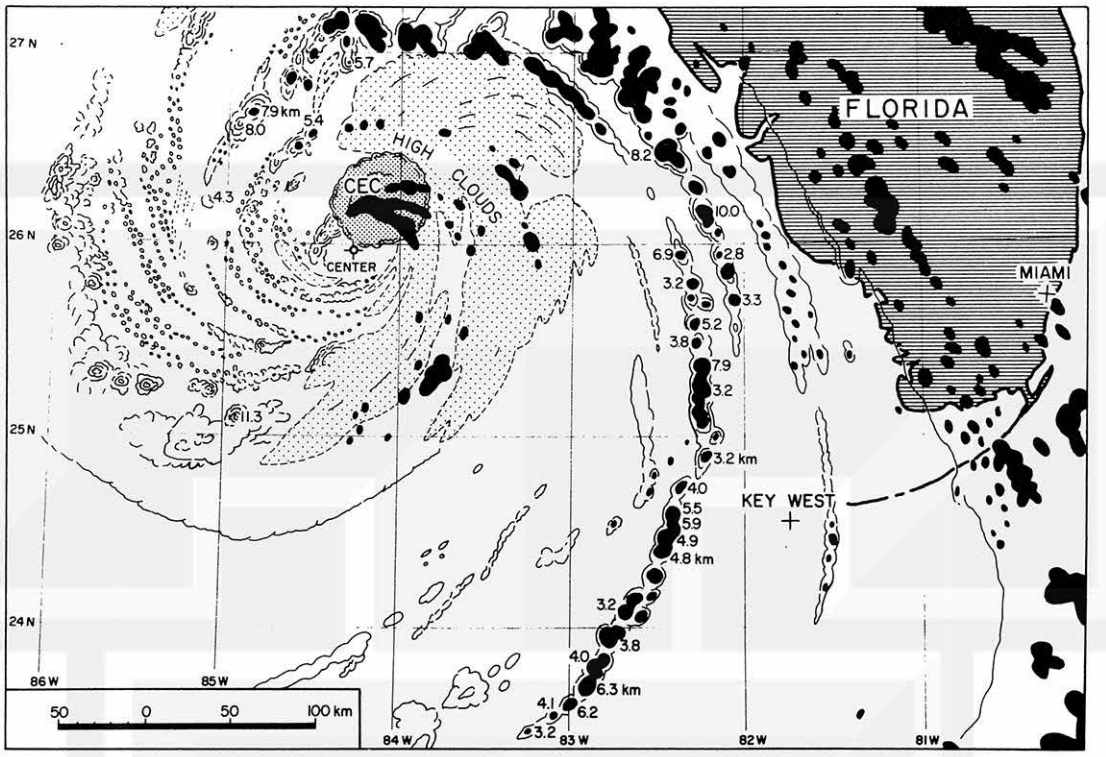

Fig. 5. An example of PPI composite echoes superimposed upon the cloud pattern derived from Apollo 7 pictures. Cloud heights shown by the echoes are in km above MSL. The height of the CEC was about 12 km at its rim.

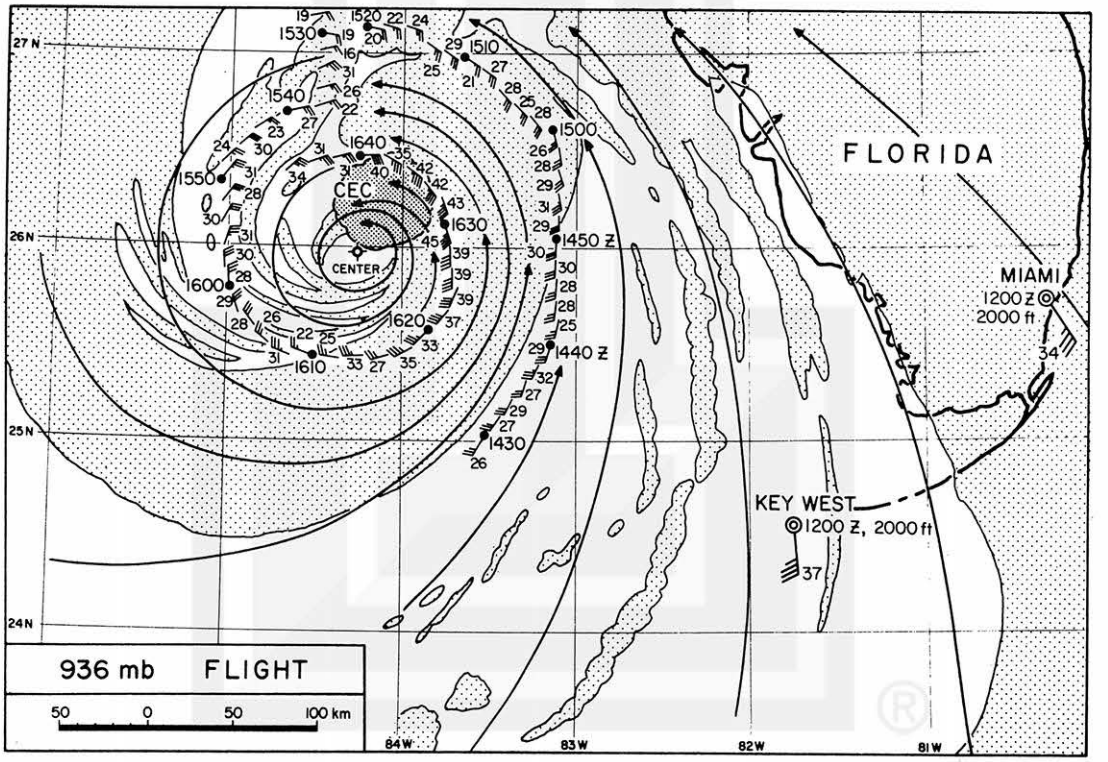

Fig. 6. Streamline analysis of winds recorded near the time of the Apollo 7 pictures on flight 681017B and superimposed on low level cloud analysis from Apollo pictures.

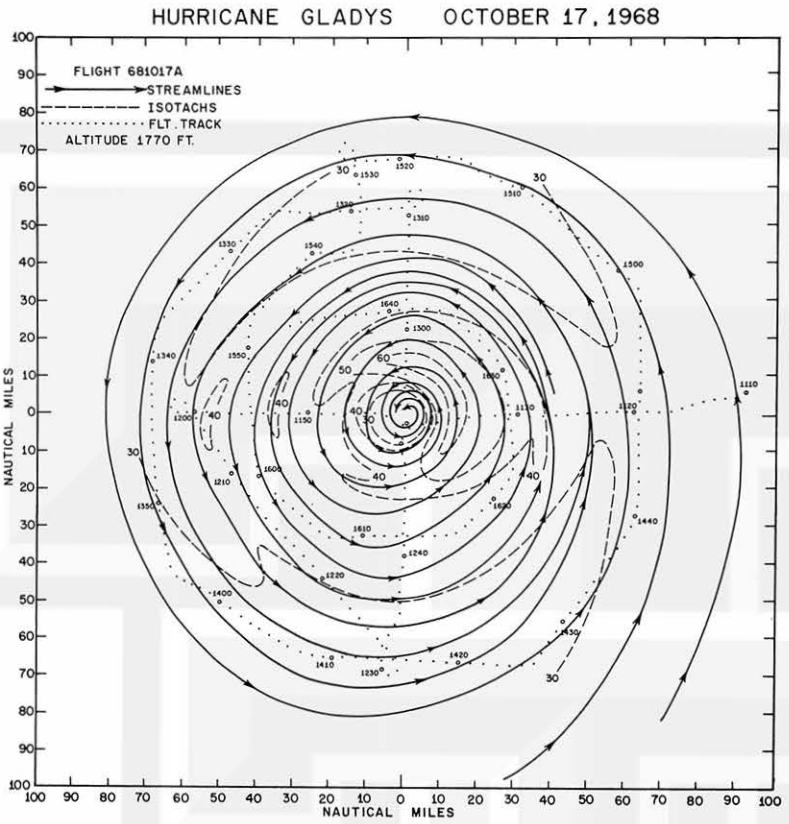

Fig. 7. Streamline and isotach analyses of winds recorded at 1770 feet on flight 681017B.

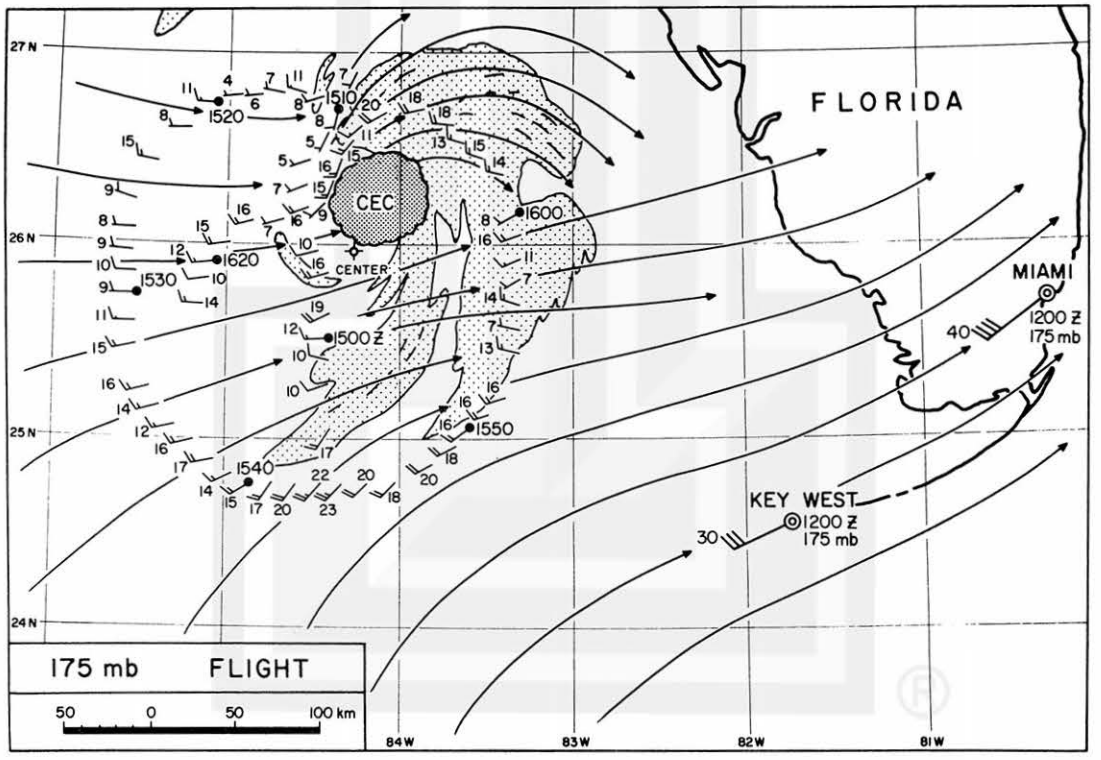

Fig. 8. Streamline analysis of winds at 44,000 feet on 17 October superimposed on high level cloud analysis from Apollo pictures.

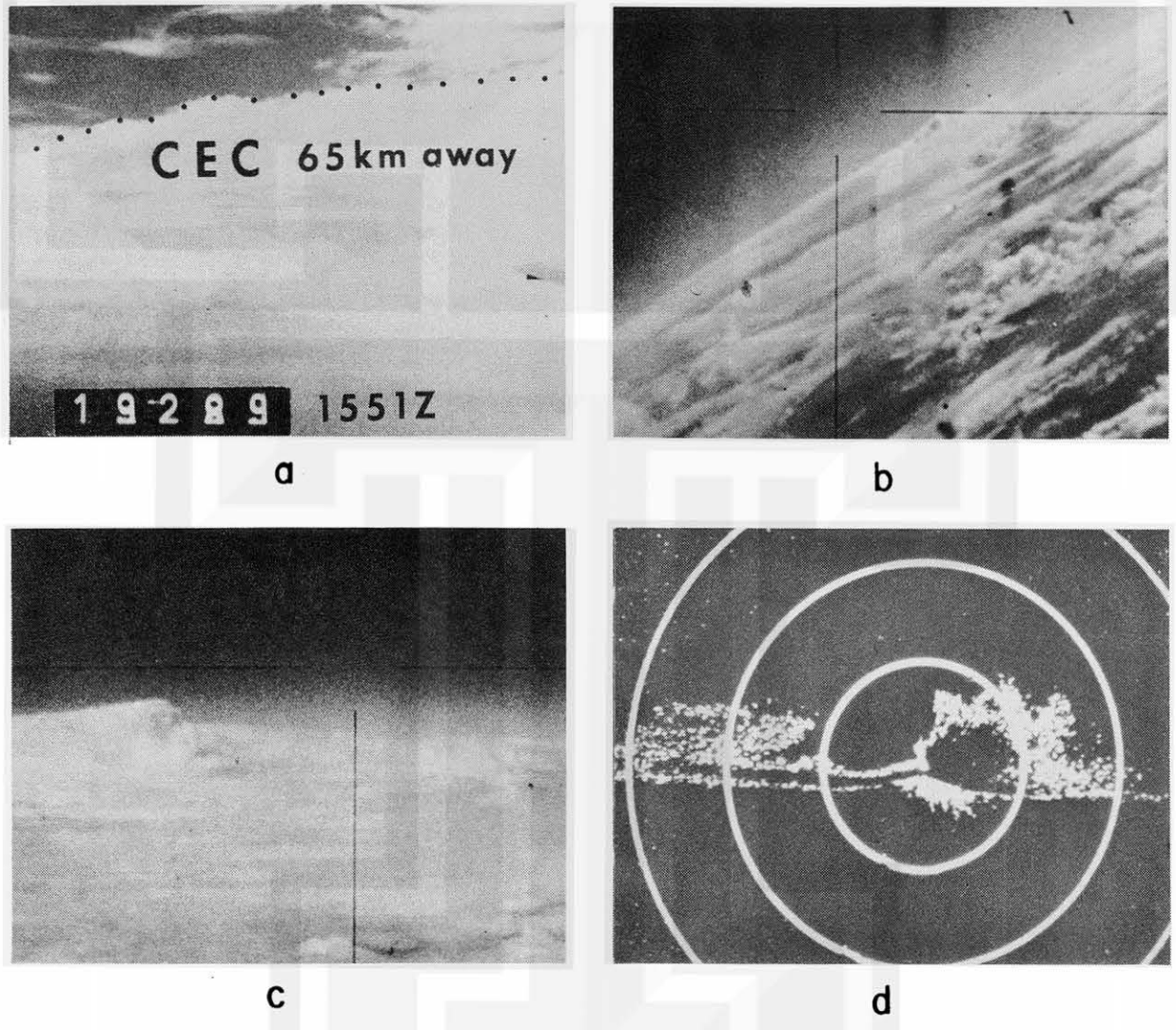

Fig. 9. Series of 4 pictures showing the CEC observed from a) DC-6 aircraft at 1551 GMT; b) B57 aircraft at 1440 GMT, c) B57 aircraft at 1452 GMT, and d) on scope of vertically oriented RDR 3.2 cm radar on DC-6 aircraft.

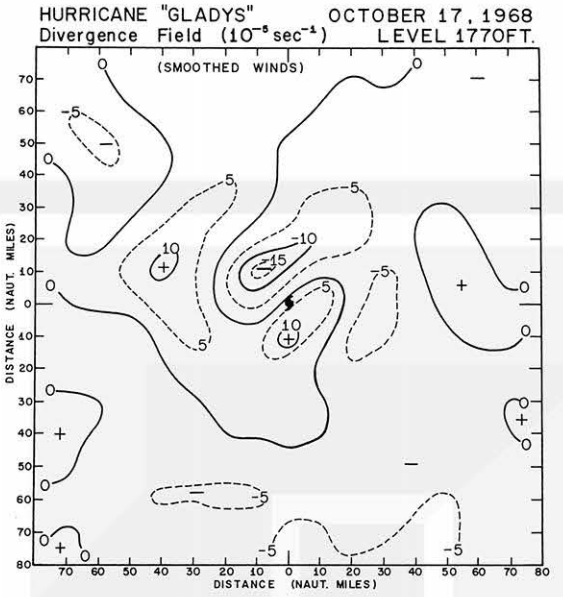

Fig. 10. Divergence field computed from smoothed aircraft aircraft winds illustrated in Figure 7.

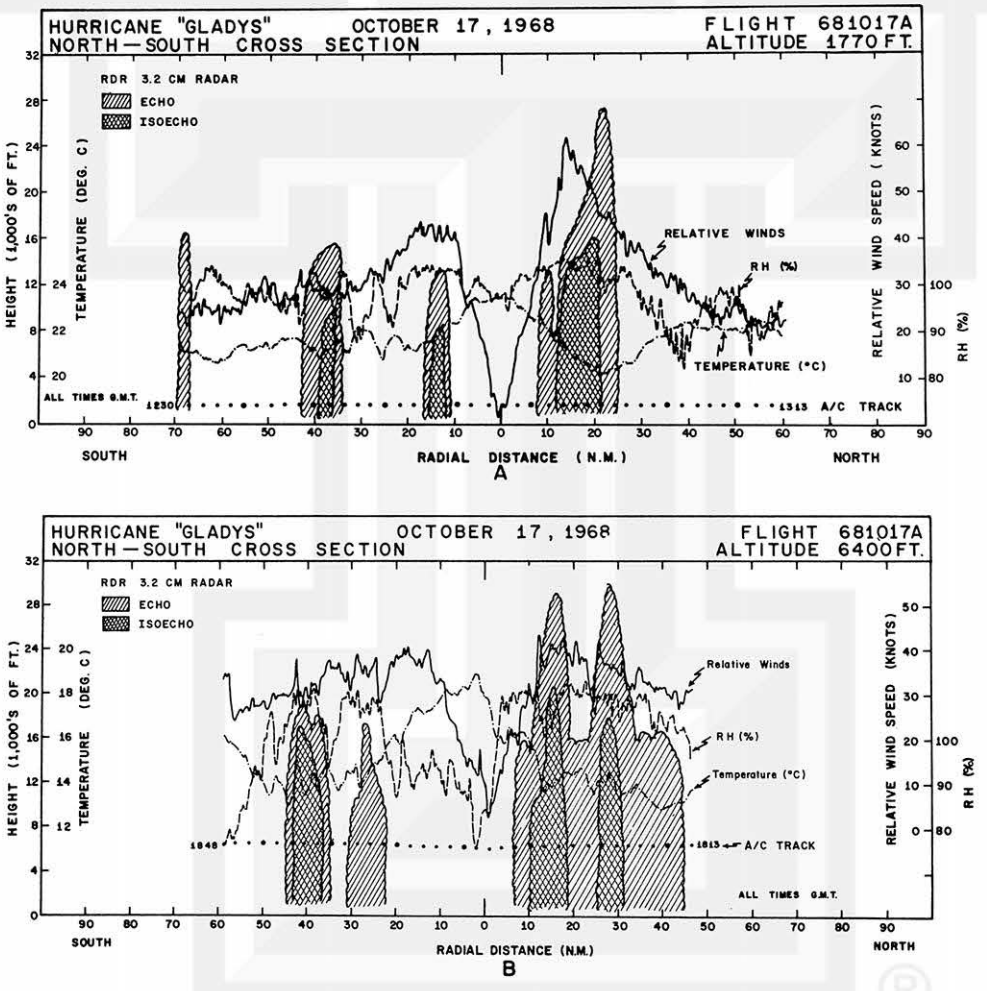

Fig. 11. A. Cross section of composite radar echoes from vertically oriented 3.2 cm radar combined with profiles of draft scale vertical motion (b only), temperature, wind speeds relative to the moving storm center, and the relative humidities for north-south oriented passes through the storm at 1230 - 1313 GMT. B. Same for 1813 - 1848 GMT. Both sections show echoes from the CEC.

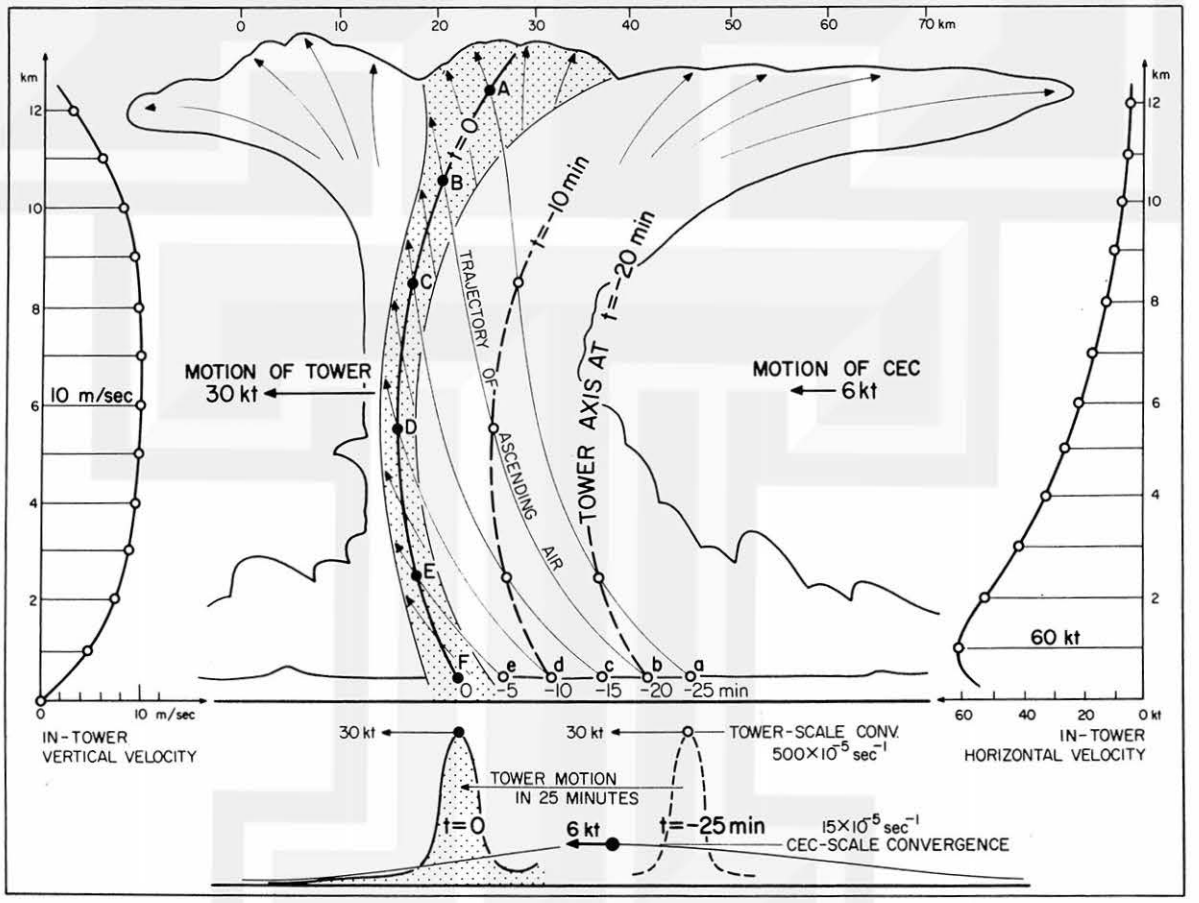

Fig. 12. A model of Circular Exhaust Cloud based on data for the CEC inside hurricane Gladys of 17 October 1968.

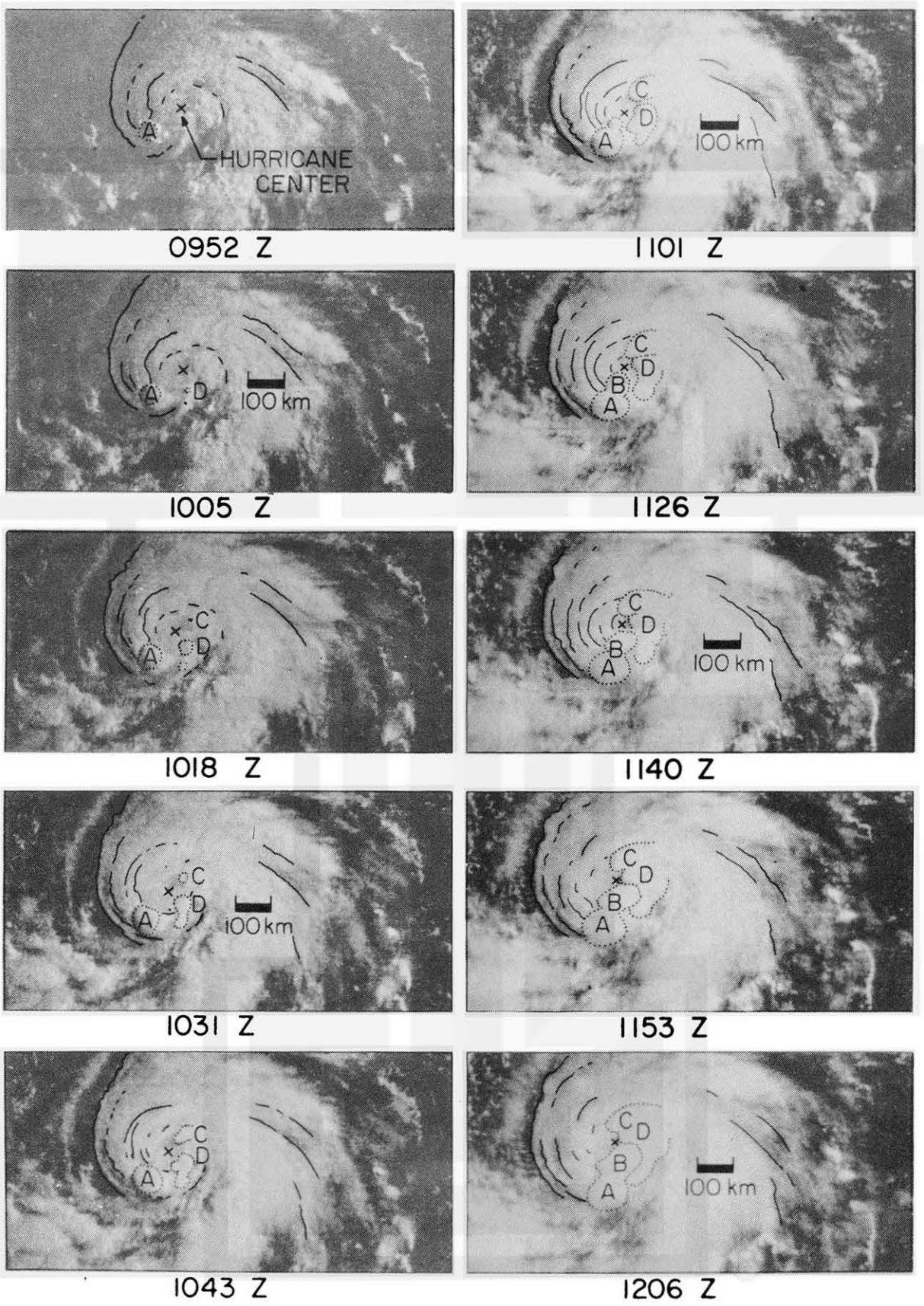

Fig. 13. Time changes in CECs seen inside hurricane Debby of 16 August 1969. Picture sequence was selected from digitized ATS-III pictures produced by NASA for Hurricane Watch Experiment, 1969.

MESOMETEOROLOGY PROJECT - - - RESEARCH PAPERS

(Continued from front cover)

42.* A Study of Factors Contributing to Dissipation of Energy in a Developing Cumulonimbus - Rodger A. Brown and Tetsuya Fujita

43. A Program for Computer Gridding of Satellite Photographs for Mesoscale Research - William D. Bonner

44. Comparison of Grassland Surface Temperatures Measured by TIROS VII and Airborne Radiometers under Clear Sky and Cirriform Cloud Conditions - Ronald M. Reap

45. Death Valley Temperature Analysis Utilizing Nimbus I Infrared Data and Ground-Based Measurements - Ronald M. Reap and Tetsuya Fujita

46. On the "Thunderstorm-High Controversy" - Rodger A. Brown

47. Application of Precise Fujita Method on Nimbus I Photo Gridding - Lt. Cmd. Ruben Nasta

48. A Proposed Method of Estimating Cloud-top Temperature, Cloud Cover, and Emissivity and Whiteness of Clouds from Short- and Long-wave Radiation Data Obtained by TIROS Scanning Radiometers - T. Fujita and H. Grandoso

49. Aerial Survey of the Palm Sunday Tornadoes of April 11, 1965 - Tetsuya Fujita

50. Early Stage of Tornado Development as Revealed by Satellite Photographs - Tetsuya Fujita

51. Features and Motions of Radar Echoes on Palm Sunday, 1965 - D. L. Bradbury and T. Fujita

52. Stability and Differential Advection Associated with Tornado Development - Tetsuya Fujita and Dorothy L. Bradbury

53. Estimated Wind Speeds of the Palm Sunday Tornadoes - Tetsuya Fujita

54. On the Determination of Exchange Coefficients: Part II - Rotating and Nonrotating Convective Currents - Rodger A. Brown

55. Satellite Meteorological Study of Evaporation and Cloud Formation over the Western Pacific under the Influence of the Winter Monsoon - K. Tsuchiya and T. Fujita

56. A Proposed Mechanism of Snowstorm Mesojet over Japan under the Influence of the Winter Monsoon - T. Fujita and K. Tsuchiya

57. Some Effects of Lake Michigan upon Squall Lines and Summertime Convection - Walter A. Lyons

58. Angular Dependence of Reflection from Stratiform Clouds as Measured by TIROS IV Scanning Radiometers - A. Rabbe

59. Use of Wet-beam Doppler Winds in the Determination of the Vertical Velocity of Raindrops inside Hurricane Rainbands - T. Fujita, P. Black and A. Loesch

60. A Model of Typhoons Accompanied by Inner and Outer Rainbands - Tetsuya Fujita, Tatsuo Izawa., Kazuo Watanabe and Ichiro Imai

61. Three-Dimensional Growth Characteristics of an Orographic Thunderstorm System - Rodger A. Brown

62. Split of a Thunderstorm into Anticyclonic and Cyclonic Storms and their Motion as Determined from Numerical Model Experiments - Tetsuya Fujita and Hector Grandoso

63. Preliminary Investigation of Peripheral Subsidence Associated with Hurricane Outflow - Ronald M. Reap

64. The Time Change of Cloud Features in Hurricane Anna, 1961, from the Easterly Wave Stage to Hurricane Dissipation - James E. Arnold

65. Easterly Wave Activity over Africa and in the Atlantic with a Note on the Intertropical Convergence Zone during Early July 1961 - James E. Arnold

66. Mesoscale Motions in Oceanic Stratus as Revealed by Satellite Data - Walter A. Lyons and Tetsuya Fujita

67. Mesoscale Aspects of Orographic Influences on Flow and Precipitation Patterns - Tetsuya Fujita

68. A Mesometeorological Study of a Subtropical Mesocyclone -Hidetoshi Arakawa, Kazuo Watanabe, Kiyoshi Tsuchiya and Tetsuya Fujita

69. Estimation of Tornado Wind Speed from Characteristic Ground Marks - Tetsuya Fujita, Dorothy L. Bradbury and Peter G. Black

70. Computation of Height and Velocity of Clouds from Dual, Whole-Sky, Time-Lapse Picture Sequences - Dorothy L. Bradbury and Tetsuya Fujita

71. A Study of Mesoscale Cloud Motions Computed from ATS-I and Terrestrial Photographs - Tetsuya Fujita, Dorothy L. Bradbury, Clifford Murino and Louis Hull

72. Aerial Measurement of Radiation Temperatures over Mt. Fuji and Tokyo Areas and Their Application to the Determination of Ground- and Water-Surface Temperatures - Tetsuya Fujita, Gisela Baralt and Kiyoshi Tsuchiya

73. Angular Dependence of Reflected Solar Radiation from Sahara Measured by TIROS VII in a Torquing Maneuver - Rene Mendez.

74. The Control of Summertime Cumuli and Thunderstorms by Lake Michigan During Non-Lake Breeze Conditions - Walter A. Lyons and John W. Wilson

75. Heavy Snow in the Chicago Area as Revealed by Satellite Pictures - James Bunting and Donna Lamb

76. A Model of Typhoons with Outflow and Subsidence Layers - Tatsuo Izawa

* out of print

(continued on outside back cover)

SATELLITE AND MESOMETEOROLOGY PROJECT - - - RESEARCH PAPERS
(Continued from inside back cover)

77. Yaw Corrections for Accurate Gridding of Nimbus HRIR Data - Roland A. Madden

78. Formation and Structure of Equatorial Anticyclones Caused by Large-Scale Cross Equatorial Flows Determined by ATS-I Photographs - Tetsuya T. Fujita and Kazuo Watanabe and Tatsuo Izawa

79. Determination of Mass Outflow From a Thunderstorm Complex Using ATS III Pictures - T. T. Fujita and D. L. Bradbury

80. Development of a Dry Line as Shown by ATS Cloud Photography and Verified by Radar and Conventional Aerological Data - Dorothy L. Bradbury

81. Dynamical Analysis of Outflow from Tornado-Producing Thunderstorms as Revealed by ATS III Pictures - K. Ninomiya

82. Computation of Cloud Heights from Shadow Positions through Single Image Photogrammetry of Apollo Pictures - T. T. Fujita